Role of Dispersive Interactions in Determining Structural Properties of Organic–Inorganic Halide Perovskites: Insights from First- Principles Calculations

ARTICLE *in* JOURNAL OF PHYSICAL CHEMISTRY LETTERS · JULY 2014

Impact Factor: 7.46 · DOI: 10.1021/jz5012934

2 AUTHORS, INCLUDING:

David Egger
Weizmann Institute of Science
25 PUBLICATIONS **199** CITATIONS

THE JOURNAL OF PHYSICAL CHEMISTRY Letters

Letter

pubs.acs.org/JPCL

Role of Dispersive Interactions in Determining Structural Properties of Organic–Inorganic Halide Perovskites: Insights from First-Principles Calculations

David A. Egger* and Leeor Kronik*

Department of Materials and Interfaces, Weizmann Institute of Science, Rehovoth 76100, Israel

ABSTRACT: A microscopic picture of structure and bonding in organic–inorganic perovskites is imperative to understanding their remarkable semiconducting and photovoltaic properties. On the basis of a density functional theory treatment that includes both spin–orbit coupling and dispersive interactions, we provide detailed insight into the crystal binding of lead–halide perovskites and quantify the effect of different types of interactions on the structural properties. Our analysis reveals that cohesion in these materials is characterized by a variety of interactions that includes important contributions from both van der Waals interactions among the halide atoms and hydrogen bonding. We also assess the role of spin–orbit coupling and show that it causes slight changes in lead–halide bonding that do not significantly affect the lattice parameters. Our results establish that consideration of dispersive effects is essential for understanding the structure and bonding in organic–inorganic perovskites in general and for providing reliable theoretical predictions of structural parameters in particular.

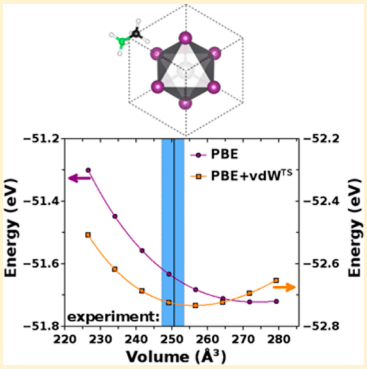

SECTION: Energy Conversion and Storage; Energy and Charge Transport

Perovskites are crystals possessing the general chemical formula ABX_3 (in which A, B, and X are ions) that adopt the calcium titanate structure. In the subclass of organic–inorganic halide perovskites (OIHPs), A is an organic cation, B is a (divalent) inorganic cation, and X is a halide anion.[1,2] In pioneering work, Mitzi and co-workers explored the exceptional properties of layered OIHPs and their potential as semiconductors in field effect transistors.[3−6] Scientific interest in these materials further intensified since the first examination of the photovoltaic properties of lead-based bulk OIHPs[7] and the discovery that their use in "meso-superstructured solar cells"[8] and in a straightforward planar heterojunction[9] can result in high-efficiency solar cells. This triggered a flurry of recent experimental[10−18] and theoretical[19−26] studies emphasizing OIHPs as candidate materials for photovoltaics and exploring their properties from different points of view.

Naively, one could expect binding and structure in perovskite-type materials to be dominated by electrostatic interactions among the different ions in the crystal. However, even distinctly ionic solids (e.g., MgO[27]) can still exhibit significant contributions from other interactions, and OIHPs in particular contain fundamentally different building blocks that can, in principle, trigger a more complex form of binding.[6] For example, following earlier work on layered OIHPs,[6] it has been suggested that hydrogen bonding between the organic molecule and inorganic cage could be important for structural determination.[19,26] Furthermore, although van der Waals (vdW) interactions are well-known in, for example, the context of rare gas, molecular, or layered crystals, the quantitative role of such interactions in the binding of covalent and ionic solids is less appreciated but has been drawing much attention recently.[28,29] Specifically, for lead–halide perovskites, Wang et al. recently demonstrated the importance of including vdW interactions in the theoretical treatment of these crystals.[30] Structure and binding in OIHPs could furthermore be affected by spin–orbit coupling (SOC), which was already shown to have a profound effect on the electronic structure of lead-based organic–inorganic perovskites.[20,22,23,25,26] To the best of our knowledge, however, an analysis that combines both dispersive interactions and SOC, allowing for the quantitative assessment of the impact of either phenomenon on the geometrical structure of OIHPs, has not been reported.

In this Letter, we provide such a quantitative understanding for lead–halide organic–inorganic perovskites on the basis of dispersion-corrected density functional theory (DFT) band structure calculations that account for SOC. We show that a careful treatment of vdW interactions is necessary for obtaining accurate geometrical structures of OIHPs and that if such interactions are indeed taken into account, very good agreement with experimental data is obtained. Furthermore, by analyzing the dispersive interactions on an atomistic level, we highlight the importance of both hydrogen bonding between the organic and inorganic parts of the material and dispersive halide–halide interactions. Furthermore, we find that inclusion of SOC somewhat modifies lead–halide bonding but does not significantly affect the lattice parameter of the crystal.

To investigate the role of dispersive interactions and SOC in OIHPs, we performed periodic DFT calculations using the

Received: June 24, 2014
Accepted: July 22, 2014
Published: July 22, 2014

   dx.doi.org/10.1021/jz5012934 | J. Phys. Chem. Lett. 2014, 5, 2728−2733

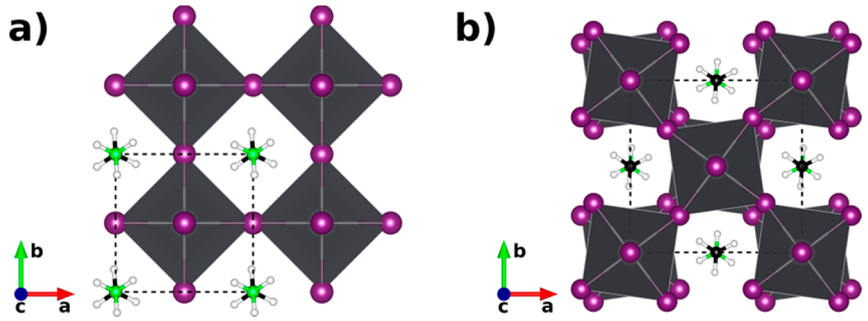

Figure 1. Schematic structural representation of $MAPbI_3$, where MA = methylammonium, in the (a) pseudocubic and (b) tetragonal phases. Thick dashed lines indicate the unit cell, which contains carbon (black), nitrogen (green), hydrogen (white), iodine (violet), and lead (light gray) atoms; the latter are inside of the dark shaded octahedra. For convenient visualization, atoms belonging to more than a standard unit cell are shown.

plane wave VASP code.[31] We employed convergence criteria of 10^{-6} eV per unit cell for the total energy in the electronic self-consistent cycle and 10^{-2} eV/Å for optimizing the forces and unit cell parameters. Two Γ-centered *k*-point grids ($8 \times 8 \times 8$ and $6 \times 6 \times 4$) have been used for the pseudocubic and tetragonal unit cells (vide infra), respectively. This allows for the two different unit cells to be mapped with similar precision in *k*-space. Core−valence electron interactions were treated within the projector-augmented wave (PAW) formalism[32] using the "normal" (i.e., not "soft") program-supplied PAW potentials. Specifically for Pb, we chose to treat the 5d electrons explicitly because they are near the 6s and 6p electrons in energy and can affect Pb covalence through exchange and correlation.[33] Unless explicitly noted otherwise, SOC effects were accounted for within the noncollinear magnetism framework of the VASP code.[34] The valence electron wave functions were expanded on a plane wave basis with a kinetic energy cutoff of 700 eV.

Exchange and correlation were treated at the generalized gradient approximation level using the Perdew−Burke−Ernzerhof (PBE) functional.[35] Generally, the electronic structure predicted from these calculations agrees well with the results of ref 22. In particular, once SOC is accounted for, the predicted band gap is ∼1 eV too small compared to experiment,[20] as expected from Kohn−Sham DFT in general.[36,37] Here, our focus is on the prediction of structural OIHP parameters. In this regard, PBE is well-known to not capture long-range dispersive interactions.[38−40] In this work, these are accounted for by adding pairwise dispersion interactions, computed using the plane wave implementation[41,42] of the Tkatchenko−Scheffler (TS) pairwise dispersion scheme,[43] to the PBE results. In this approach, which we denote as PBE+vdW^{TS} in the following, the PBE-computed total energy of the system is augmented by pairwise vdW energies E_{vdW}^{AB} calculated for each atomic pair AB using vdW parameters (density-scaled atomic polarizabilities, C_6 coefficients, and vdW radii) that are obtained from a Hirshfeld partitioning[44] of the self-consistently computed PBE charge density.[43,45,46]

We start our examination by focusing on the most commonly studied OIHP, methylammonium-lead-iodide, in which A = methylammonium (MA), B = lead, and X = iodine ($MAPbI_3$). Depending on temperature, $MAPbI_3$ crystallizes in several phases that are characterized by different crystal structures. Here, we focus on two phases of $MAPbI_3$, one of which is pseudocubic (i.e., possessing almost equal lattice constants along the three axes) with one $MAPbI_3$ unit per unit cell, and the other is tetragonal with four $MAPbI_3$ units per cell.[47] Both structures are shown in Figure 1.

For the conceptually simpler pseudocubic phase (Figure 1a), we optimized the lattice parameters by performing explicit calculations for the energy as a function of volume. We used an experimentally determined structure[47] as a starting point, imposed the experimentally observed pseudocubic ratio of the unit cell vectors, and minimized the forces on the atoms while keeping the unit cell vectors fixed for a set of eight volumes that span roughly ±10% of the experimentally reported volume of the unit cell. Importantly, here and throughout, we use the shortcomings of PBE with respect to dispersive interactions to our advantage because a comparison of calculations with and without dispersive corrections exposes the importance of these interactions directly.[48,49] The results of this comparison are given in Figure 2.

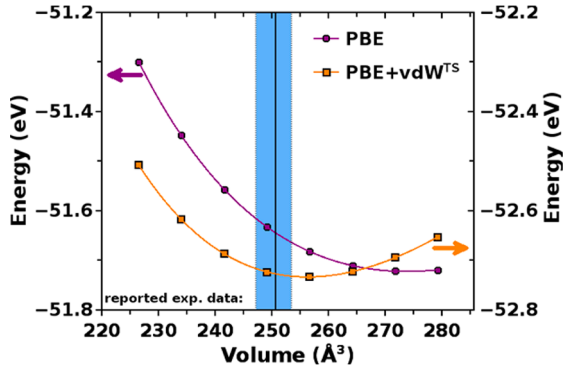

Figure 2. Total energy as a function of volume for pseudocubic $MAPbI_3$ using PBE (purple circles) and PBE+vdW^{TS} (orange squares). The vertical line and blue-shaded area denote the mean value and lower/higher limit of experimentally reported values (see Table 1), respectively.

Interestingly, comparison of the two energy−volume curves in Figure 2 immediately reveals that the structure of $MAPbI_3$ is strongly affected by dispersive interactions, resulting in a significant contraction of the unit cell volume (by ∼18 Å^3). Most importantly, only the minimum volume extracted from the PBE+vdW^{TS} calculations (obtained from a Murnaghan[50,51] fit to the energy−volume curves) is in satisfactory agreement with experimental volumes reported in the literature (see Figure 2 and Table 1). Naturally, this dispersion-corrected result also manifests itself in the optimized lattice constants (see Table 1), which exhibit a difference of only 0.04 Å from the experimental mean value as compared with a much larger

dx.doi.org/10.1021/jz5012934 | J. Phys. Chem. Lett. 2014, 5, 2728−2733

Table 1. Calculated Structural Parameters[a,b] of (Pseudo-) Cubic Lead−Halide Organic−Inorganic Perovskites, Compared to Experimental Data[18,47,55,56]

		a (Å)	b (Å)	c (Å)	V (Å^3)
$MAPbI_3$	experiment 1[47]	6.31	6.31	6.32	251.6
	experiment 2[55]	6.33			253.5
	experiment 3[56]	6.28			247.1
	PBE$^{E(V)\text{-opt}}$	6.49	6.49	6.50	273.8
	PBE+vdW$^{TS,E(V)\text{-opt}}$	6.35	6.35	6.36	256.3
	PBE$^{\text{direct-opt,400 eV}}$	6.38	6.38	6.38	259.7
	PBE$^{\text{direct-opt}}$	6.48	6.48	6.49	272.3
	PBE+vdW$^{TS,\text{direct-opt}}$	6.35	6.35	6.35	255.9
	PBE$^{\text{direct-opt,no-SOC}}$	6.47	6.47	6.48	271.3
$MAPbBr_3$	experiment 1[18]	5.94			209.6
	experiment 2[55]	5.90			206.3
	PBE	6.08			224.6
	PBE+vdW^{TS}	5.97			213.0
$MAPbCl_3$	experiment[55]	5.68			182.8
	PBE	5.81			196.2
	PBE+vdW^{TS}	5.71			186.2

[a]Lattice constants and unit cell volume. [b]"PBE+vdW^{TS}" and "PBE" denote calculations with and without explicit inclusion of dispersive interactions, respectively. "$E(V)$-opt" and "direct-opt" denote structural relaxations via energy−volume curves or via direct optimization using the stress tensor, respectively. The additional superscripts "400 eV" and "no-SOC" denote that our default settings for kinetic energy cutoff and inclusion of SOC were modified deliberately; see text for details.

0.18 Å difference from the mean experimental value without dispersion corrections. These finding are in line with ref 30, where it was shown in SOC-free calculations that neglecting vdW interactions leads to overestimated lattice parameters of OIHPs. Here, it is shown that this conclusion stands even when SOC is incorporated.

To ensure that this conclusion does not depend on the internal details of the TS scheme, we have performed additional PBE+vdW^{TS} calculations based on an iterative Hirshfeld partitioning of the density.[29] In this approach, effective volumes, polarizabilities, and C_6 coefficients are calculated based on a self-consistently determined, possibly ionic reference system, as opposed to the necessarily neutral atoms in the standard Hirshfeld scheme.[29] For the pseudocubic $MAPbI_3$, we found that this increased the average C_6 coefficient for I by ∼22% and decreased it for Pb by ∼59%. Nevertheless, structural predictions did not change dramatically, with the pseudocubic lattice constant slightly increasing to 6.39 Å, that is, 0.08 Å away from experiment. This relative insensitivity is consistent with similar observations in ref 29, where it was attributed to partial cancellation between increasing effective volumes and stronger short-range damping of the dispersion interaction. In light of this, only the usual TS scheme is used henceforth.

Energy−volume optimizations are cumbersome in practice, especially when calculating more complex structural phases of perovskites. Therefore, we tested whether the same level of accuracy can be achieved in a more straightforward manner, that is, by a direct force and stress relaxation of $MAPbI_3$. To this end, we employed the GADGET[52] optimizer, which relies on internal coordinates. This often results in improved convergence, compared to conventional optimization schemes, and also allows one to constrain the lattice vectors to their experimentally determined ratio in a natural manner, which we employed to facilitate comparison between experiment and theory.

In Table 1, we compare the calculated lattice parameters of $MAPbI_3$ optimized with two different kinetic energy cutoffs (400 and 700 eV) at the PBE level (i.e., without including vdW). Using the lower cutoff energy (400 eV) in direct force and stress optimization results in a volume of the pseudocubic phase that is smaller by 14 Å^3 compared to the volume extracted above, with lattice vectors that are more than 0.1 Å smaller. We note that without the attractive contribution from dispersive interactions, the energy−volume dependence can be much weaker, which renders numerical convergence in direct stress and force optimizations more difficult.[53,54] Indeed, the bulk modulus of pseudocubic $MAPbI_3$, computed by fitting the energy−volume dependence with the Murnaghan expression, increased from 10.3 to 15.3 GPa upon adding the TS dispersive corrections. Therefore, we have explicitly verified that the weaker energy−volume dependence with PBE does not compromise our stress relaxation by using a larger unit cell as a starting point in the direct optimization. Only when increasing the cutoff energy (to 700 eV) did the directly optimized lattice parameters converge toward the ones retrieved from explicit energy−volume optimization, finally differing by less than 0.01 Å.

The unphysical contraction of the unit cell is due to spurious stress components associated with representing a variable size unit cell with an incomplete basis set, making the direct stress relaxation optimization more susceptible to finite basis set errors than the energy minimization approach[57,58] (note that here we followed the standard procedure of maintaining a constant plane wave cutoff energy during each volume optimization). These two approaches generally lead to different results for the lattice parameters, unless full convergence with respect to the plane wave cutoff energy is achieved.[57,58] This is particularly challenging in the case of $MAPbI_3$ as, due to the presence of the organic molecule in the crystal, variations in the atomic distances are relatively large. Our results therefore indicate that the use of a small cutoff energy in a direct stress optimization spuriously reduces the unit cell dimensions. This, coupled with the neglect of dispersion interactions that tend to reduce unit cell dimensions, results in cancellation of errors that could lead to fortuitous agreement with experiment (cf. Table 1). These findings may help in understanding some discrepancies among PBE-based calculations for structural parameters of OIHPs, reported in recent literature (e.g., compare the significantly different lattice parameters reported for pseudocubic $MAPbI_3$ in refs 22 and 26). Note, however, that these considerations do not rule out other causes of discrepancy between theory and experiment, for example, insufficiently accurate approximations for the choice of the exchange−correlation functional, dispersion correction scheme (especially the neglect of many-body dispersion[46]), and numerical solution strategy, or further refinement in the interpretation of the experimental results.

With a reliable direct optimization procedure at hand, we can easily assess the crystal structure of other OIHPs, $MAPbBr_3$ and $MAPbCl_3$. These results are also given in Table 1. As in the case of $MAPbI_3$, again dispersive interactions are responsible for a significant contraction of the unit cell, correcting for the otherwise too large volume predicted by PBE and again leading to good agreement with experimental data. We further considered the more complex and equally relevant tetragonal phase of $MAPbI_3$ (see Figure 1b). The results, given in Table 2,

dx.doi.org/10.1021/jz5012934 | J. Phys. Chem. Lett. 2014, 5, 2728−2733

Table 2. Calculated Structural Parameters[a,b] of Tetragonal $MAPbI_3$, Compared to Experimental Data[47,55,56]

	a (Å)	b (Å)	c (Å)	V (Å^3)
experiment 1[47]	8.85		12.64	990.0
experiment 2[55]	8.86		12.66	992.6
experiment 3[56]	8.85		12.44	975.0
PBE	9.04		12.92	1056.4
PBE+vdW^{TS}	8.89		12.70	1003.9

[a]Lattice constants and unit cell volume. [b]"PBE+vdW^{TS}" and "PBE" denote calculations with and without explicitly including dispersive interactions, respectively.

confirm that also for this phase, dispersive interactions have a significant effect on the lattice parameters and are therefore absolutely crucial for reliable structural optimizations.

In addition to structural prediction, the above calculations also provide us with insights into the chemical nature of the pertinent dispersive interactions. This is achieved by quantifying the strength of the different pairwise interactions through explicit calculation of the energy contribution, E_{vdW}^{AB}, of each atom−site pair, AB, in the unit cell of the (pseudo)cubic phases of $MAPbX_3$ (X = I, Br, Cl). The result is given in Figure 3a. Note that due to the periodicity of the system, E_{vdW}^{AB} can be finite even for A = B as this corresponds to the interaction of two atoms in different unit cells that occupy the same site within the cell. By definition for a pairwise dispersive energy term, $E_{vdW}^{AB} = E_{vdW}^{BA}$. Therefore, to prevent double counting, each pair is counted only once in the total energy, as reflected graphically in Figure 3a. The results summarized graphically in Figure 3a show that the leading dispersive contribution in lead−halide perovskites stems from direct vdW interaction between the halides. For $MAPbI_3$, these energies amount up to ∼0.1 eV per atomic pair, which is indeed in the range of typical vdW energies. Clearly, the large polarizability of the halogen atoms induces sizable vdW interactions in the halide octahedron of the OIHPs. Consistent with this interpretation, these interactions get weaker in the expected order of iodine, bromine, and chlorine, reducing to ∼50 meV per bond for the latter.

It was furthermore suggested that hydrogen bonding is important for OIHPs.[19,26] This notion is also supported by the results of Figure 3a. In the case of the pseudocubic phase of $MAPbI_3$, the halide−hydrogen bonds contribute a dispersive pairwise energy of up to ∼17 meV per bond, which counting all relevant hydrogen interactions amounts to a dispersive energy of ∼0.25 eV per unit cell, again in the range typical for such interactions. Importantly, this should not be taken as the full extent of the strength of the hydrogen bond. Unlike in vdW interactions, which are virtually absent in a PBE calculation, the nondispersive part of the hydrogen bond is known to be reasonably described by PBE.[45,46,59] Still, our results do indicate that even the missing dispersive element alone is non-negligible here. The importance of the overall hydrogen bonding is also revealed through the fully optimized pseudocubic $MAPbI_3$ structure, shown in Figure 3b. The figure clearly shows a preferred orientation of the MA unit, such that it is "locked in" so as to optimize hydrogen−halide distances for hydrogen bonding. We find this preferred orientation of MA also for the cases of $MAPbBr_3$ and $MAPbCl_3$, for which the nondispersive part of hydrogen bonding is more relevant than that in the case of $MAPbI_3$ because the electronegativity of Br and especially Cl is larger than that of I.

Finally, we consider the effect of SOC. While it has already been shown to affect the electronic structure of OIHPs strongly,[20,22] its impact on the geometrical structure has, to the best of our knowledge, not been assessed so far. We examine its effect by using PBE+vdW^{TS} for pseudocubic $MAPbI_3$ with SOC contributions explicitly switched off in the optimization of the crystal. The obtained optimized unit cell volume and relaxed lattice constants (see Table 1) are virtually identical to those obtained with SOC interactions. However, we find that the Pb−I bond lengths along the c-axis of the pseudocubic crystal somewhat change without SOC, with the main effect being a

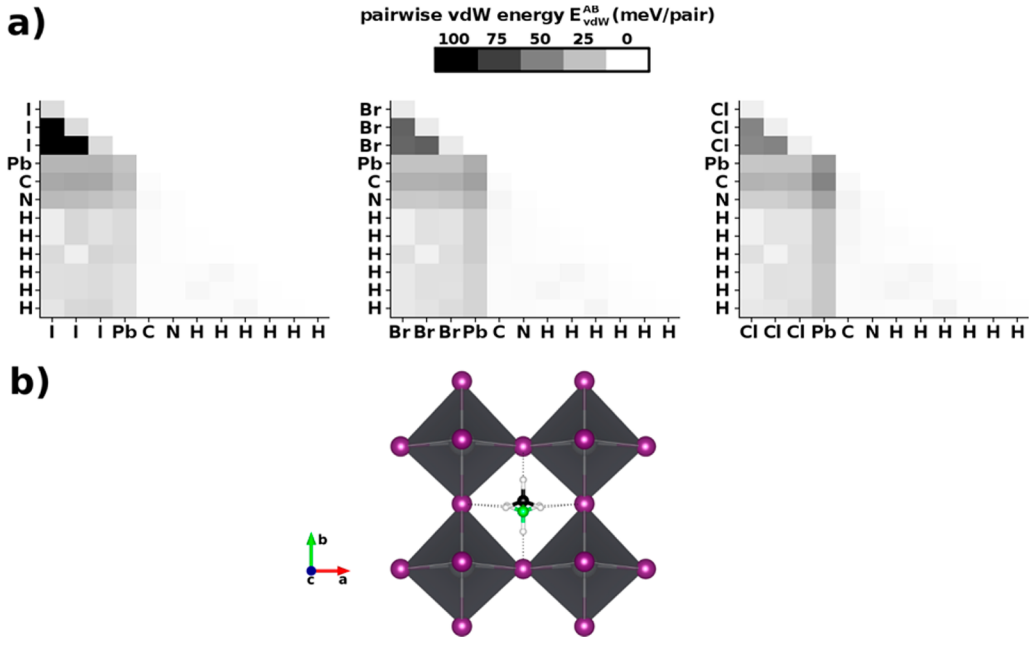

Figure 3. (a) Graphical summary of pairwise vdW energies, E_{vdW}^{AB}, between atom sites A and B in the unit cell of $MAPbI_3$ (left panel), $MAPbBr_3$ (center panel), and $MAPbCl_3$ (right panel). (b) Optimized structure of pseudocubic $MAPbI_3$, with the thin dashed lines indicating hydrogen bonds.

dx.doi.org/10.1021/jz5012934 | J. Phys. Chem. Lett. 2014, 5, 2728−2733

slightly smaller difference (by 0.05 Å) in the two Pb−I bond lengths along the *c*-axis. This variation in the Pb−I bonds is due to small movements of the Pb atom along the *c*-axis, which hardly affects the lattice constants. We note that this small variation in the geometry only changes the energy very weakly and is therefore at the limit of numerical accuracy achievable within our computational scheme.

In conclusion, we have analyzed the importance of different types of interactions relevant to the structure and bonding of organic−inorganic perovskites from first principles based on a DFT treatment that explicitly includes both SOC and pairwise dispersion interactions. Our most important finding is that crystal binding in these materials is characterized by a variety of interactions that extends beyond purely covalent/ionic bonding and includes significant contributions from both vdW interactions among the halide atoms and hydrogen bonding. We have also assessed the role of SOC in determination of structural parameters and showed that it may cause slight changes in lead−halide bond lengths that do not significantly affect the lattice parameters. Our results clearly demonstrate that consideration of dispersive effects is essential for understanding the structure and bonding in organic−inorganic perovskites in general and for providing reliable theoretical predictions of structural parameters in particular.

AUTHOR INFORMATION

Corresponding Authors

*E-mail: david.egger@weizmann.ac.il (D.A.E.).
*E-mail: leeor.kronik@weizmann.ac.il (L.K.).

Notes

The authors declare no competing financial interest.

ACKNOWLEDGMENTS

We thank David Cahen, Gershom Martin, Eran Edri, and Andrew M. Rappe for illuminating discussions. Research was supported by the Leona M. and Harry B. Helmsley Charitable Trust and by the Lise Meitner Minerva Center for Computational Chemistry.

REFERENCES

(1) Snaith, H. J. Perovskites: The Emergence of a New Era for Low-Cost, High-Efficiency Solar Cells. *J. Phys. Chem. Lett.* **2013**, *4*, 3623−3630.

(2) Hodes, G. Perovskite-Based Solar Cells. *Science* **2013**, *342*, 317−318.

(3) Mitzi, D. B.; Feild, C. A.; Harrison, W. T. A.; Guloy, A. M. Conducting Tin Halides with a Layered Organic-Based Perovskite Structure. *Nature* **1994**, *369*, 467−469.

(4) Mitzi, D. B.; Wang, S.; Feild, C. A.; Chess, C. A.; Guloy, A. M. Conducting Layered Organic-Inorganic Halides Containing ⟨110⟩-Oriented Perovskite Sheets. *Science* **1995**, *267*, 1473−1476.

(5) Kagan, C. R.; Mitzi, D. B.; Dimitrakopoulos, C. D. Organic−Inorganic Hybrid Materials as Semiconducting Channels in Thin-Film Field-Effect Transistors. *Science* **1999**, *286*, 945−947.

(6) Mitzi, D. B. Synthesis, Structure, and Properties of Organic−Inorganic Perovskites and Related Materials. In *Progress in Inorganic Chemistry*; Karlin, K. D., Ed.; John Wiley & Sons, Inc.: Hoboken, NJ, 1999; Vol. *48*, pp 1−121.

(7) Kojima, A.; Teshima, K.; Shirai, Y.; Miyasaka, T. Organometal Halide Perovskites as Visible-Light Sensitizers for Photovoltaic Cells. *J. Am. Chem. Soc.* **2009**, *131*, 6050−6051.

(8) Lee, M. M.; Teuscher, J.; Miyasaka, T.; Murakami, T. N.; Snaith, H. J. Efficient Hybrid Solar Cells Based on Meso-Superstructured Organometal Halide Perovskites. *Science* **2012**, *338*, 643−647.

(9) Liu, M.; Johnston, M. B.; Snaith, H. J. Efficient Planar Heterojunction Perovskite Solar Cells by Vapour Deposition. *Nature* **2013**, *501*, 395−398.

(10) Stranks, S. D.; Eperon, G. E.; Grancini, G.; Menelaou, C.; Alcocer, M. J.; Leijtens, T.; Herz, L. M.; Petrozza, A.; Snaith, H. J. Electron−Hole Diffusion Lengths Exceeding 1 Micrometer in an Organometal Trihalide Perovskite Absorber. *Science* **2013**, *342*, 341−344.

(11) Burschka, J.; Pellet, N.; Moon, S.-J.; Humphry-Baker, R.; Gao, P.; Nazeeruddin, M. K.; Grätzel, M. Sequential Deposition as a Route to High-Performance Perovskite-Sensitized Solar Cells. *Nature* **2013**, *499*, 316−319.

(12) Heo, J. H.; Im, S. H.; Noh, J. H.; Mandal, T. N.; Lim, C.-S.; Chang, J. A.; Lee, Y. H.; Kim, H.; Sarkar, A.; Nazeeruddin, M. K.; et al. Efficient Inorganic−Organic Hybrid Heterojunction Solar Cells Containing Perovskite Compound and Polymeric Hole Conductors. *Nat. Photonics* **2013**, *7*, 486−491.

(13) Marchioro, A.; Teuscher, J.; Friedrich, D.; Kunst, M.; van de Krol, R.; Moehl, T.; Grätzel, M.; Moser, J.-E. Unravelling the Mechanism of Photoinduced Charge Transfer Processes in Lead Iodide Perovskite Solar Cells. *Nat. Photonics* **2014**, *8*, 250−255.

(14) Edri, E.; Kirmayer, S.; Cahen, D.; Hodes, G. High Open-Circuit Voltage Solar Cells Based on Organic−Inorganic Lead Bromide Perovskite. *J. Phys. Chem. Lett.* **2013**, *4*, 897−902.

(15) Edri, E.; Kirmayer, S.; Kulbak, M.; Hodes, G.; Cahen, D. Chloride Inclusion and Hole Transport Material Doping to Improve Methyl Ammonium Lead Bromide Perovskite-Based High Open-Circuit Voltage Solar Cells. *J. Phys. Chem. Lett.* **2014**, *5*, 429−433.

(16) Edri, E.; Kirmayer, S.; Henning, A.; Mukhopadhyay, S.; Gartsman, K.; Rosenwaks, Y.; Hodes, G.; Cahen, D. Why Lead Methylammonium Tri-Iodide Perovskite-Based Solar Cells Require a Mesoporous Electron Transporting Scaffold (but Not Necessarily a Hole Conductor). *Nano Lett.* **2014**, *14*, 1000−1004.

(17) Edri, E.; Kirmayer, S.; Mukhopadhyay, S.; Gartsman, K.; Hodes, G.; Cahen, D. Elucidating the Charge Carrier Separation and Working Mechanism of $CH_3NH_3PbI_{3-x}Cl_x$ Perovskite Solar Cells. *Nat. Commun.* **2014**, *5*, 3461.

(18) Noh, J. H.; Im, S. H.; Heo, J. H.; Mandal, T. N.; Seok, S. I. Chemical Management for Colorful, Efficient, and Stable Inorganic−Organic Hybrid Nanostructured Solar Cells. *Nano Lett.* **2013**, *13*, 1764.

(19) Mosconi, E.; Amat, A.; Nazeeruddin, M. K.; Grätzel, M.; De Angelis, F. First-Principles Modeling of Mixed Halide Organometal Perovskites for Photovoltaic Applications. *J. Phys. Chem. C* **2013**, *117*, 13902−13913.

(20) Even, J.; Pedesseau, L.; Jancu, J.-M.; Katan, C. Importance of Spin−Orbit Coupling in Hybrid Organic/Inorganic Perovskites for Photovoltaic Applications. *J. Phys. Chem. Lett.* **2013**, *4*, 2999−3005.

(21) Brivio, F.; Walker, A. B.; Walsh, A. Structural and Electronic Properties of Hybrid Perovskites for High-Efficiency Thin-Film Photovoltaics from First-Principles. *APL Mater.* **2013**, *1*, 042111.

(22) Giorgi, G.; Fujisawa, J.-I.; Segawa, H.; Yamashita, K. Small Photocarrier Effective Masses Featuring Ambipolar Transport in Methylammonium Lead Iodide Perovskite: A Density Functional Analysis. *J. Phys. Chem. Lett.* **2013**, *4*, 4213−4216.

(23) Brivio, F.; Butler, K. T.; Walsh, A.; van Schilfgaarde, M. Relativistic Quasiparticle Self-Consistent Electronic Structure of Hybrid Halide Perovskite Photovoltaic Absorbers. *Phys. Rev. B* **2014**, *89*, 155204.

(24) Frost, J. M.; Butler, K. T.; Brivio, F.; Hendon, C. H.; van Schilfgaarde, M.; Walsh, A. Atomistic Origins of High-Performance in Hybrid Halide Perovskite Solar Cells. *Nano Lett.* **2014**, *14*, 2584.

(25) Umari, P.; Mosconi, E.; De Angelis, F. Relativistic GW Calculations on $CH_3NH_3PbI_3$ and $CH_3NH_3SnI_3$ Perovskites for Solar Cell Applications. *Sci. Rep.* **2014**, *4*, 4467.

(26) Amat, A.; Mosconi, E.; Ronca, E.; Quarti, C.; Umari, P.; Nazeeruddin, M. K.; Grätzel, M.; De Angelis, F. Cation-Induced Band-Gap Tuning in Organohalide Perovskites: Interplay of Spin−Orbit Coupling and Octahedra Tilting. *Nano Lett.* **2014**, *14*, 3608.

(27) Doll, K.; Dolg, M.; Fulde, P.; Stoll, H. Correlation Effects in Ionic Crystals: The Cohesive Energy of MgO. *Phys. Rev. B* **1995**, *52*, 4842.
(28) Zhang, G.-X.; Tkatchenko, A.; Paier, J.; Appel, H.; Scheffler, M. Van Der Waals Interactions in Ionic and Semiconductor Solids. *Phys. Rev. Lett.* **2011**, *107*, 245501.
(29) Bučko, T.; Lebègue, S.; Hafner, J.; Ángyán, J. G. Improved Density Dependent Correction for the Description of London Dispersion Forces. *J. Chem. Theory Comput.* **2013**, *9*, 4293−4299.
(30) Wang, Y.; Gould, T.; Dobson, J. F.; Zhang, H.; Yang, H.; Yao, X.; Zhao, H. Density Functional Theory Analysis of Structural and Electronic Properties of Orthorhombic Perovskite $CH_3NH_3PbI_3$. *Phys. Chem. Chem. Phys.* **2014**, *16*, 1424.
(31) Kresse, G.; Furthmüller, J. Efficient Iterative Schemes for Ab Initio Total-Energy Calculations Using a Plane-Wave Basis Set. *Phys. Rev. B* **1996**, *54*, 11169−11186.
(32) Kresse, G.; Joubert, D. From Ultrasoft Pseudopotentials to the Projector Augmented-Wave Method. *Phys. Rev. B* **1999**, *59*, 1758−1775.
(33) Walsh, A.; Payne, D. J.; Egdell, R. G.; Watson, G. W. Stereochemistry of Post-Transition Metal Oxides: Revision of the Classical Lone Pair Model. *Chem. Soc. Rev.* **2011**, *40*, 4455.
(34) Hobbs, D.; Kresse, G.; Hafner, J. Fully Unconstrained Noncollinear Magnetism within the Projector Augmented-Wave Method. *Phys. Rev. B* **2000**, *62*, 11556.
(35) Perdew, J. P.; Burke, K.; Ernzerhof, M. Generalized Gradient Approximation Made Simple. *Phys. Rev. Lett.* **1996**, *77*, 3865−3868.
(36) Perdew, J. P.; Levy, M. Physical Content of the Exact Kohn−Sham Orbital Energies: Band Gaps and Derivative Discontinuities. *Phys. Rev. Lett.* **1983**, *51*, 1884.
(37) Sham, L.; Schlüter, M. Density-Functional Theory of the Energy Gap. *Phys. Rev. Lett.* **1983**, *51*, 1888.
(38) Langreth, D. C.; Lundqvist, B. I.; Chakarova-Käck, S. D.; Cooper, V. R.; Dion, M.; Hyldgaard, P.; Kelkkanen, A.; Kleis, J.; Kong, L.; Li, S.; et al. A Density Functional for Sparse Matter. *J. Phys.: Condens. Matter* **2009**, *21*, 084203.
(39) Riley, K. E.; Pitoňák, M.; Jurečka, P.; Hobza, P. Stabilization and Structure Calculations for Noncovalent Interactions in Extended Molecular Systems Based on Wave Function and Density Functional Theories. *Chem. Rev.* **2010**, *110*, 5023−5063.
(40) Klimeš, J.; Michaelides, A. Perspective: Advances and Challenges in Treating van Der Waals Dispersion Forces in Density Functional Theory. *J. Chem. Phys.* **2012**, *137*, 120901.
(41) Al-Saidi, W. A.; Voora, V. K.; Jordan, K. D. An Assessment of the vdW-TS Method for Extended Systems. *J. Chem. Theory Comput.* **2012**, *8*, 1503−1513.
(42) Bučko, T.; Lebègue, S.; Hafner, J.; Ángyán, J. Tkatchenko−Scheffler van Der Waals Correction Method with and without Self-Consistent Screening Applied to Solids. *Phys. Rev. B* **2013**, *87*, 064110.
(43) Tkatchenko, A.; Scheffler, M. Accurate Molecular Van Der Waals Interactions from Ground-State Electron Density and Free-Atom Reference Data. *Phys. Rev. Lett.* **2009**, *102*, 073005.
(44) Hirshfeld, F. L. Bonded-Atom Fragments for Describing Molecular Charge Densities. *Theor. Chim. Acta* **1977**, *44*, 129−138.
(45) Marom, N.; Tkatchenko, A.; Rossi, M.; Gobre, V. V.; Hod, O.; Scheffler, M.; Kronik, L. Dispersion Interactions with Density-Functional Theory: Benchmarking Semiempirical and Interatomic Pairwise Corrected Density Functionals. *J. Chem. Theory Comput.* **2011**, *7*, 3944−3951.
(46) Kronik, L.; Tkatchenko, A. Understanding Molecular Crystals with Dispersion-Inclusive Density Functional Theory: Pairwise Corrections and Beyond. *Acc. Chem. Res.* **2014**, DOI: 10.1021/ar500144s.
(47) Stoumpos, C. C.; Malliakas, C. D.; Kanatzidis, M. G. Semiconducting Tin and Lead Iodide Perovskites with Organic Cations: Phase Transitions, High Mobilities, and Near-Infrared Photoluminescent Properties. *Inorg. Chem.* **2013**, *52*, 9019−9038.
(48) Egger, D. A.; Ruiz, V. G.; Saidi, W. A.; Bučko, T.; Tkatchenko, A.; Zojer, E. Understanding Structure and Bonding of Multilayered Metal−Organic Nanostructures. *J. Phys. Chem. C* **2013**, *117*, 3055−3061.
(49) Azuri, I.; Adler-Abramovich, L.; Gazit, E.; Hod, O.; Kronik, L. Why Are Diphenylalanine-Based Peptide Nanostructures so Rigid? Insights from First Principles Calculations. *J. Am. Chem. Soc.* **2014**, *136*, 963−969.
(50) Murnaghan, F. D. The Compressibility of Media under Extreme Pressures. *Proc. Natl. Acad. Sci. U.S.A.* **1944**, *30*, 244−247.
(51) Fu, C.-L.; Ho, K.-M. First-Principles Calculation of the Equilibrium Ground-State Properties of Transition Metals: Applications to Nb and Mo. *Phys. Rev. B* **1983**, *28*, 5480.
(52) Bučko, T.; Hafner, J.; Ángyán, J. G. Geometry Optimization of Periodic Systems Using Internal Coordinates. *J. Chem. Phys.* **2005**, *122*, 124508.
(53) Bučko, T.; Hafner, J.; Lebègue, S.; Ángyán, J. G. Improved Description of the Structure of Molecular and Layered Crystals: Ab Initio DFT Calculations with van Der Waals Corrections. *J. Phys. Chem. A* **2010**, *114*, 11814−11824.
(54) Voora, V. K.; Al-Saidi, W. A.; Jordan, K. D. Density Functional Theory Study of Pyrophyllite and M-Montmorillonites (M = Li, Na, K, Mg, and Ca): Role of Dispersion Interactions. *J. Phys. Chem. A* **2011**, *115*, 9695−9703.
(55) Poglitsch, A.; Weber, D. Dynamic Disorder in Methylammoniumtrihalogenoplumbates (II) Observed by Millimeter-Wave Spectroscopy. *J. Chem. Phys.* **1987**, *87*, 6373.
(56) Baikie, T.; Fang, Y.; Kadro, J. M.; Schreyer, M.; Wei, F.; Mhaisalkar, S. G.; Graetzel, M.; White, T. J. Synthesis and Crystal Chemistry of the Hybrid Perovskite $(CH_3NH_3)PbI_3$ for Solid-State Sensitised Solar Cell Applications. *J. Mater. Chem. A* **2013**, *1*, 5628.
(57) Francis, G. P.; Payne, M. C. Finite Basis Set Corrections to Total Energy Pseudopotential Calculations. *J. Phys.: Condens. Matter* **1990**, *2*, 4395.
(58) Dacosta, P. G.; Nielsen, O. H.; Kunc, K. Stress Theorem in the Determination of Static Equilibrium by the Density Functional Method. *J. Phys. C: Solid State Phys.* **1986**, *19*, 3163.
(59) Koch, W.; Holthausen, M. C. *A Chemist's Guide to Density Functional Theory*; Wiley-VCH: Weinheim, Germany; New York, 2001.